Electrochimica Acta 518 (2025) 145776

Contents lists available at ScienceDirect

Electrochimica Acta

journal homepage: www.journals.elsevier.com/electrochimica-acta

Does Pb underpotential deposition rearrange surface-near atoms in AgAu films and nanoparticles?

Dean-Robin Nettler [a], Jan Clausmeyer [a], Alan Savan [b], Paolo Cignoni [a], Christian Rurainsky [a], Ralf Drautz [c], Alfred Ludwig [b], Kristina Tschulik [a,d,*]

[a] Ruhr University Bochum, Faculty of Chemistry and Biochemistry, Chair of Analytical Chemistry II, Bochum, Germany
[b] Ruhr University Bochum, Faculty of Mechanical Engineering, Chair of Materials Discovery and Interfaces, Bochum, Germany
[c] Ruhr University Bochum, Interdisciplinary Centre for Advanced Materials Simulation, Department of Atomistic Modelling and Simulation, Bochum, Germany
[d] Max-Planck-Institut für Nachhaltige Materialien GmbH, Max-Planck-Straße 1, 40237 Düsseldorf, Germany

ARTICLE INFO

Keywords:
AgAu alloy
Underpotential deposition
Combinatorial sputtering
Surface modification

ABSTRACT

Bimetallic surfaces consisting of Ag and Au in various ratios, as sputtered thin films as well as wet-chemically synthesised nanoparticles were modified by underpotential deposition of Pb (Pb-UPD). On the basis of characteristic voltametric peaks along with supporting DFT calculations we conclude that depositing Pb on the Ag-rich surfaces induces a swap of Ag atoms with underlying Au atoms to form a Au-rich layer in the presence of the Pb monolayer. Our experiments showed that Pb-UPD is a powerful tool not only to probe the surface composition and structure but to change the arrangement of surface atoms in binary alloys.

1. Introduction

Underpotential deposition (UPD) is a quantitative method commonly used to characterise electrocatalytic surfaces, particularly regarding their electrochemically active surface area, by using cyclic voltammetry (CV) [1–8]. Furthermore, it allows the determination of energetic and structural aspects of 2D phase formations [9]. In UPD, a metal that is less noble than the metal(s) on the surface under study is electrochemically deposited at potentials that are less negative than required for bulk electrodeposition of the less noble metal [10–12]. For instance, Pb can be deposited on Au(111) at a potential positive of its nominal deposition potential as a monolayer, because Pb^{2+} ions need less energy to be deposited on Au(111) than is required for their deposition on a Pb crystal. For this reason, the deposition of Pb stops after the formation of a monolayer and is only continued at a significantly more negative potential, where "overpotential deposition" takes place [8,13]. While forming a Pb monolayer on a Au(111) surface, the Pb monolayer/adlayer shows a hexagonal close packed (hcp) structure [14,15]. Accordingly, measuring the amount of Pb deposited on an electrode during UPD can be used to measure its electrochemically available surface area [16,17]. The potential required for UPD strongly depends on both the electrode material and its crystallographic orientation. Hence, Pb-UPD takes place at less negative potentials on Au(100) than on Au(111) surfaces [9]. On (100) surfaces UPD is influenced by monoatomic steps on metal substrates, where it is adsorbed preferentially. On (111) surfaces these Pb superlattice structures were not observed [9]. Furthermore, the deposition potential of Pb on different metals is specific. This characteristic is helpful for the separation of monolayer deposition on a binary alloy such as Ag_xAu_y. The Ag_xAu_y system is an ideal model system for solid solutions as the binary system is completely miscible. In this system the required potential for Pb-UPD on Au is more positive than on Ag. Subsequent to the UPD the Pb monolayer is usually oxidised, which leads to a reconstruction of the original surface with slight differences in the topography [14].

In some cases, adlayers deposited by UPD become involved in rearrangements of surface-near atoms. For instance, the less noble metal deposited by UPD can form an alloy with the original metal substrate, which restructures the original metal surface. For example, Shin et al. reported, that Pb-UPD at different sweep rates on a Au surface led to the formation of surface alloys. Slower sweep rates of Pb-UPD resulted in a more heavily alloyed surface than UPD with faster sweep rates since the hcp adlayer has more time to transform into the alloy structure [18]. Another example is the UPD of Sb on Au. Such experiments led to a structural transition that exposed Au islands in the Sb monolayer [19]. Another example is monolayered Ag by Ag-UPD on Au with subsequent Pb-UPD leads to positively shifted Ag oxidation peaks during stripping,

* Corresponding author at: Ruhr University Bochum, Faculty of Chemistry and Biochemistry, Chair of Analytical Chemistry II, Bochum, Germany.
E-mail address: Kristina.Tschulik@rub.de (K. Tschulik).

https://doi.org/10.1016/j.electacta.2025.145776
Received 7 August 2024; Received in revised form 22 January 2025; Accepted 28 January 2025
Available online 29 January 2025

while samples not treated with Pb-UPD do not show such behaviour [20].

In this work, we explore to what extent UPD can be used as a tool to purposefully manipulate the structure of alloy surfaces. In previous works, we have characterised Ag_xAu_y nanoparticles with different compositions using anodic stripping voltammetry and Pb-UPD. The determined nanoparticle size, configuration and surface composition were confirmed by several other analytical methods, yet they did not indicate the formation of a Pb surface alloy [16,21,22]. Here we investigate whether this difference to the previously reported behaviour of Au macroelectrodes originates from the nanoparticulate or the alloy character of the samples. Hence, we compare Pb-UPD on different Ag_xAu_y alloy nanoparticles with complementary thin film samples. To this end, Ag_xAu_y thin films are prepared as materials libraries by combinatorial sputtering. This technique can be used to form thin films with well-defined composition gradients by co-deposition from multiple metal sources or alternatively by multilayer deposition of nanoscale wedges. Materials libraries prepared using co-sputtering comprise typically compositions from 20 to 80 at.% for binary systems [23]. Combinatorial sputtering has been used for high-throughput screening of multi-component functional alloys and allows us to compare Ag_xAu_y film samples with compositions similar to that of the used Ag_xAu_y nanoparticles [24].

Thus, we demonstrate that Pb-UPD is a sensitive method to probe the surface composition of binary alloys, namely combinatorially sputtered thin films and chemically synthesised nanoparticles. Furthermore, we show that it is possible to change the surface composition of Ag_xAu_y alloys due to adsorption and desorption of Pb monolayers. This rearrangement of Ag_xAu_y surfaces results from a change of Ag and Au atom positions in the presence of Pb, while no hint for the formation of a ternary surface alloy was found.

2. Experimental section

2.1. Thin film deposition

The Ag_xAu_y thin film samples were prepared by magnetron sputtering in an ultra-high vacuum (UHV) deposition system (CMS 600/400 LIN, DCA Instruments, Finland) on a Si(100) wafer with a Ti adhesion layer. The apparatus consists of a loadlock, UHV central distribution chamber with a robot for substrate movement, and 2 UHV magnetron sputtering deposition chambers. Pre-cut pieces of (100) Si with a 500 nm SiO_2 barrier layer were used as substrates. Immediately before deposition of the binary film, a 15 nm thick adhesion layer of Ti (Goodfellow, 99.99 %) was deposited in PVD chamber 1, then transferred in UHV to the confocal cathodes chamber 2.

This chamber has 5 confocal 100 mm diameter cathodes positioned 72° apart from each other and tilted 45° relative to the plane of the substrate. The centre-to-centre target to substrate distance is about 187 mm. When the substrate is constantly rotated during deposition, a film of uniform thickness is grown from arriving species that are atomically mixed in the gas phase prior to condensation. In this way, uniform thin films of Ag and Au were also made, for comparison. Elemental targets with 100 mm diameter were placed on each cathode: Ag (KJ Lesker, 99.99 %), Au (Sindlhauser, 99.99 %). The starting pressure was 2.4×10^{-6} Pa and there was no intentional heating used. Each target was precleaned by sputtering against individual, closed shutters, then the film was grown at a pressure of 0.67 Pa of pure Ar (99.9999 %) with the substrates being static thus forming composition spread films (materials libraries). Each cathode had a separate generator, with the power applied to each being adjusted to achieve the desired film composition gradients.

2.2. Scanning electron microscopy

Scanning electron microscopy (SEM) X-ray dispersive spectroscopy (EDX) was performed to determine the compositions of the sputtered samples. This was done on a JEOL 5800 SEM at 20 kV acceleration voltage in 10 mm working distance, a magnification of 600x with an INCA X-act EDS detector (Oxford Instruments), and data collection time of 60 s was chosen. The data was analysed using INCA software (Oxford Instruments), with quantification calibration done with a pre-measured Co standard.

2.3. X-ray diffraction

X-ray powder diffraction (XRD) patterns were recorded on a Bruker D8 Discover (Bruker Corporation) with Bragg-Bretano geometry. The Cu-Kα beam size was collimated to 1 mm and the sample to detector distance was 149 mm (collimator diameter of 1 mm with a divergence of $<0.007°$). A VANTEC-500 area detector was used to collect the diffraction data using offset scans to avoid the substrate peaks. The diffraction data were integrated to 1D diffractograms using DIFFRAC. EVA software (Bruker Corporation).

2.4. Electrochemical characterisation of thin film samples

The thin film Ag_xAu_y alloy samples made by combinatorial sputtering showed a gradient of increasing Ag content in one direction and a gradient of increasing Au content in the opposite direction (see Fig. 3A). The material libraries were cut in six pieces of the same size to yield six samples each with a different ratio of Ag to Au. Each piece was inserted in a cell with a diameter of d = 6 mm for UPD (see SI Figure S5). These samples served as a working electrode (WE) and a graphite rod (d = 6 mm) was used as a counter electrode (CE). As a reference electrode (RE) a mercury-mercurous sulphate electrode (MSE, $E = 658$ mV vs. standard hydrogen electrode (SHE) [25], SI analytics GmbH) was used. For Pb-UPD a deoxygenated (Ar-saturated) 0.1 M NaOH solution (≥98 % ACS grade, VWR chemicals) + 1 mM $Pb(NO_3)_2$ (99,999 % trace metal basis, Riedel-de-Haen) in ultra-pure water (ThermoFisher Scientific Barnstead Gen-Pure xCAD Plus, conductivity: ≤0.055 μS/cm at 25 °C) was used. The chosen potential range was between −0.43 V and −1.16 V vs. MSE at a scan rate of 0.1 V/s for nanoparticles and 0.05 V/s for thin film samples. Five cycles were measured in each case. The figures displayed in this work consistently show the third cycle.

2.5. Nanoparticle synthesis

Ag_xAu_y nanoparticles were synthesised according to a protocol by Grasmik *et al.* [16] based on the synthesis route by Turkevich *et al.* [26]. In this synthesis route, the precursor solutions were first added to degassed, boiling water at 100 °C and immediately afterwards trisodium citrate dihydrate was added while the solution was vigorously stirred in the flask. The reaction mixture was stirred for 60 min at 100 °C under reflux and subsequently cooled to room temperature with an ice bath. In the next step, the capping agent was exchanged by adding Polyvinylpyrrolidone (PVP) and stirring overnight at room temperature. The nanoparticle suspension was centrifuged, washed with ultra-pure water and the supernatant above the nanoparticles was removed with a pipette.

The compositions of these nanoparticle systems were determined by EDX and confirmed by atomic absorption spectrometry (AAS) and CV (for detailed characterisation data see reference [16]).

2.6. Electrochemical characterisation of the nanoparticle samples

The Ag_xAu_y nanoparticles were electrochemically characterised using a glassy carbon (GC) electrode (diameter d = 4,0 mm) as a WE. This electrode was polished beforehand with Al_2O_3 particle suspensions in three different sizes (1 μm, 0.3 μm, and 0.05 μm from LECO Instruments GmbH) for 3 min each. Next, the GC electrodes were sonicated for 3 min in a sonication bath (Elma Elmasonic S100H). 2 μl of the

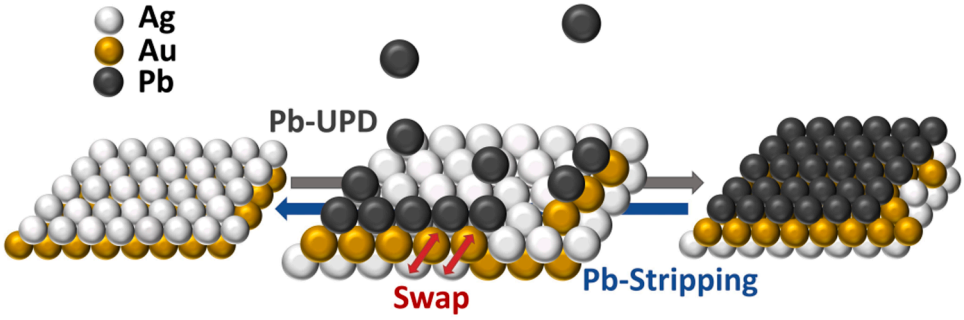

Fig. 1. Schematic visualisation of Pb-UPD on Ag_xAu_y alloys. Upon Pb-UPD, Ag surface atoms swap positions with underlying Au atoms. This process is reversed when the Pb is removed again.

Ag_xAu_y nanoparticle suspension was drop-cast onto the WE and was then dried under Ar flow. These electrochemical experiments were conducted with the same RE and CE and with the same procedures as for the non-nanoparticle samples.

All electrochemical measurements were performed with a AutoLab PGStat 12 potentiostat and all voltammograms displayed in this work are referenced against the standard hydrogen electrode (SHE).

3. Results and discussion

In a previous study we conducted an in-depth analysis of the Ag_xAu_y nanoparticles used in this work [16]. To characterise the particle composition, size, elemental distribution, morphology, and crystallinity, data from a range of techniques is available: UV–Vis, AAS, SEM, transmission electron microscopy (TEM), EDX, atomic force microscope (AFM), XRD, dynamic light scattering (DLS), differential centrifugal sedimentation (DCS) as well as anodic stripping CV and UPD (see [16]).

In this present work the analyses of monometallic Ag and Au nanoparticles are also included to offer a comparison to the binary metallic nanoparticles. These nanoparticles were tested for UPD and it was revealed that the deposition and stripping potentials for Pb on the monometallic materials is distinct from the binary ones. Hence, signals for Ag and Au nanoparticles can be clearly separated (Fig. 2A), which is important to distinguish the position of the peak potential for Pb deposition/stripping in the binary case [15,16,27]. Especially for Au, two different surface exposed facets can be identified with Pb-UPD on the basis of two distinct peaks in the CV [16,28–30]. Pb deposition and stripping peaks from Au surfaces of nanoparticle systems depend on the surface-exposed facets, that is the particle shape. For Au nanoparticles associated with Au(111) facets, a split stripping peak at around −0.35 V vs. SHE is observed, while a single peak at −0.33 V vs. SHE is measured from spherical nanoparticles [15,29,31]. In a previous work we performed Pb-UPD on Ag_xAu_y nanoparticles and found that Pb deposition occurs mainly on Ag atoms. This is in line with reports that Ag commonly forms the outermost layer of Ag_xAu_y alloy particles in aquoxes solution [32].

Investigating the stripping of Pb after Pb-UPD on such Ag_xAu_y nanoparticles, we observe that Pb is stripped from Au atoms, not from Ag atoms in the present work. As the UPD deposition peak still indicates a deposition onto Ag atoms, Ag and Au atoms apparently swap their positions once Pb atoms are deposited on the outermost layer, as detailed next.

Fig. 2A shows Pb-UPD signals recorded for monometallic Ag and Au nanoparticles synthesised via the same route and capping agent as used for Ag_xAu_y nanoparticle synthesis. Pb deposition peaks are observed at −0.21 V and at −0.35 V vs. SHE, indicating the presence of both Au(110) and Au(111) surface-exposed facets. The associated stripping peaks can be observed at −0.32 V vs. SHE for Au(111) and −0.16 V vs. SHE for Au (110). The CV of the Pb-UPD for monometallic Ag nanoparticles shows a deposition peak at −0.42 V and Pb stripping of −0.36 V vs. SHE [16].

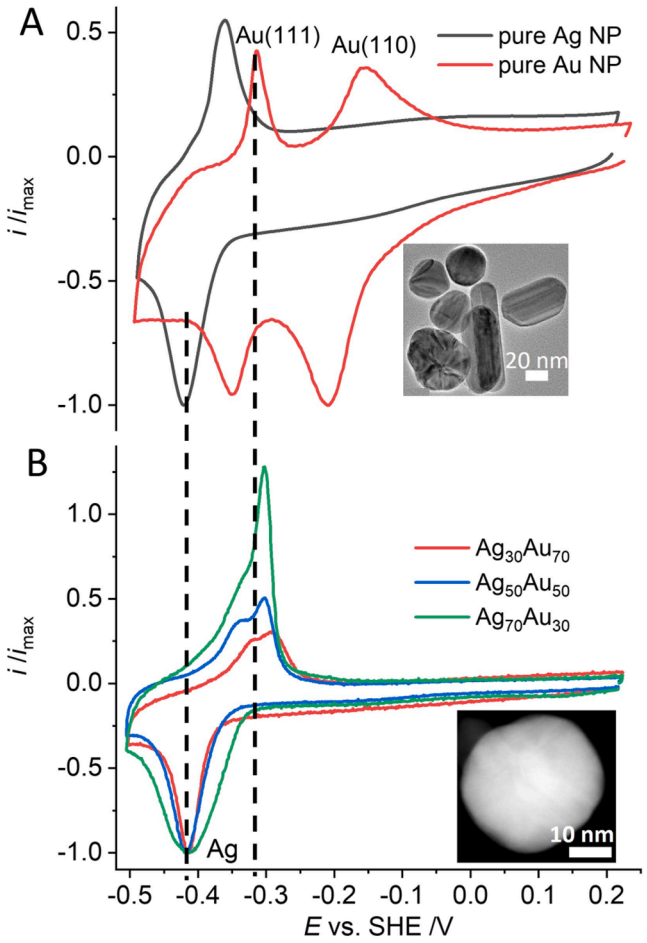

Fig. 2. CVs for Pb-UPD on different nanoparticles A) Ag and Au B) Ag_xAu_y nanoparticles (shown in the TEM images) with three compositions. All measurements were conducted in 1 mM $Pb(NO_3)_2$ + 0.1 M NaOH at a scan rate of 0.1 V/s.

Next Pb-UPD of Ag_xAu_y nanoparticles with different compositions was conducted. The detected peaks for the binary metallic nanoparticles (Fig. 2B) are assigned to the formation of a Pb monolayer on a Ag surface (−0.42 V vs. SHE). This finding reveals an alloy configuration of a Ag shell – Au core nanoparticle system, which was previously confirmed by TEM-EDX analysis, in line with theoretical predictions [32,33]. In contrast, the Pb stripping peak of the Ag_xAu_y nanoparticles occurred at around −0.30 V vs. SHE which is consistent with oxidation of the Pb layer from an Au(111) surface (Fig. 2B). This observation indicates a replacement of Ag atoms by Au atoms from an underlying layer.

To see if this effect was specific to the nanoscopic size of the particles or reproducible on other Ag_xAu_y systems with a different morphology, we performed Pb-UPD on Ag_xAu_y thin film samples. First, the Pb-UPD of the pure metal film samples is discussed to enable the assignment of the peak potentials occurring for the binary films. As shown in Fig. 3B, the Ag film shows a Pb deposition peak at −0.45 V while the Pb oxidation peak is observed at −0.35 V vs. SHE. The Pb-UPD on Au films (Fig. 3B) shows Pb deposition at −0.36 V and a stripping peak at −0.29 V vs. SHE. Given the strong (111) texture of the polycrystalline Au film (see SI Figure S2 for XRD data showing this), these Pb deposition and stripping peaks can be assigned to a Au(111) surface. It is well-known in the literature that Ag and Au are perfectly miscible at room temperature, which strongly indicates the formation of an alloy in the bulk material [34]. Ag_xAu_y alloys do not conform to the linearity of Vegard's law and show lattice parameters with distinct negative deviations compared to the pure metals. This was also found in our lattice parameters calculated from X-ray diffractograms for the thin films (see SI Figure S3) and for the nanoparticles (see reference [16]), which agree with previously reported lattice parameters of binary Ag_xAu_y alloys [35,36].

To study Ag_xAu_y film samples with different compositions but otherwise identical properties, we used a Ag_xAu_y compositional library. The compositions of the six measured samples ranged from about $Ag_{73}Au_{27}$ to about $Ag_{40}Au_{60}$, as determined by EDX analysis. UPD experiments were performed in a cylindrical electrochemical cell, exposing a geometric area of 0.028 mm^2 of each film sample to the Pb-containing electrolyte.

The resulting Pb-UPD voltammograms are displayed in Fig. 3C. The sample with the highest Ag content (≈73 % Ag, sample 1), showed a Pb deposition peak at around −0.44 V vs. SHE. This indicates Pb deposition onto a Ag surface, given that Pb-UPD onto monometallic Ag films was detected at −0.45 V vs. SHE. The deposition peaks on Ag cannot be assigned to one specific crystal facet, as the UPD potential of distinct crystal facets are very similar for Ag [16,28].

With increasing Au content in the Ag_xAu_y film samples, the Pb deposition peak shifts slightly to more positive potentials. Yet, it remains characteristic of Pb deposition on an Ag, rather than on an Au surface. We conclude that all samples, including the Au-rich ones, expose an outermost atomic layer predominantly consisting of Ag.

However, the Pb stripping peak of these CVs (e.g. −0.31 V vs. SHE for the most Ag rich sample, sample 1) can be assigned to a monolayer of Pb on Au(111) (−0.29 V vs. SHE) [15,37]. With increasing Au content in the alloy thin films (from sample 1 to sample 6), the Pb stripping peak (at around −0.30 V vs. SHE) successively shifts in the positive direction and becomes broader. This broadening is attributable to the appearance of a second peak, caused by Pb oxidation from a crystal facet different from the predominant Au(111) plane. For instance, for Pb-UPD CVs from polycrystalline Au surfaces, it is known that the stripping from an Au (100) surface appears about 100 mV more positive than that from Au (111) surfaces [15]. This crystal facet was neither observed in the spherical monometallic Au nanoparticle sample nor in binary nanoparticles [16,28]. We assume that the Pb oxidation peaks we detect for Au-rich films are a combination of the Pb stripping from Au(111) and from Au(100) facets, originating from a partial restructuring of the surface upon Pb deposition.

The CV results seen for the binary metallic nanoparticles and for the films suggest that the surface of the films and nanoparticles initially consists predominantly of Ag, and then Ag atoms are replaced by Au atoms from underlying layers upon electrochemical deposition of a Pb monolayer [16,28]. This postulated mechanism is illustrated in Fig. 1.

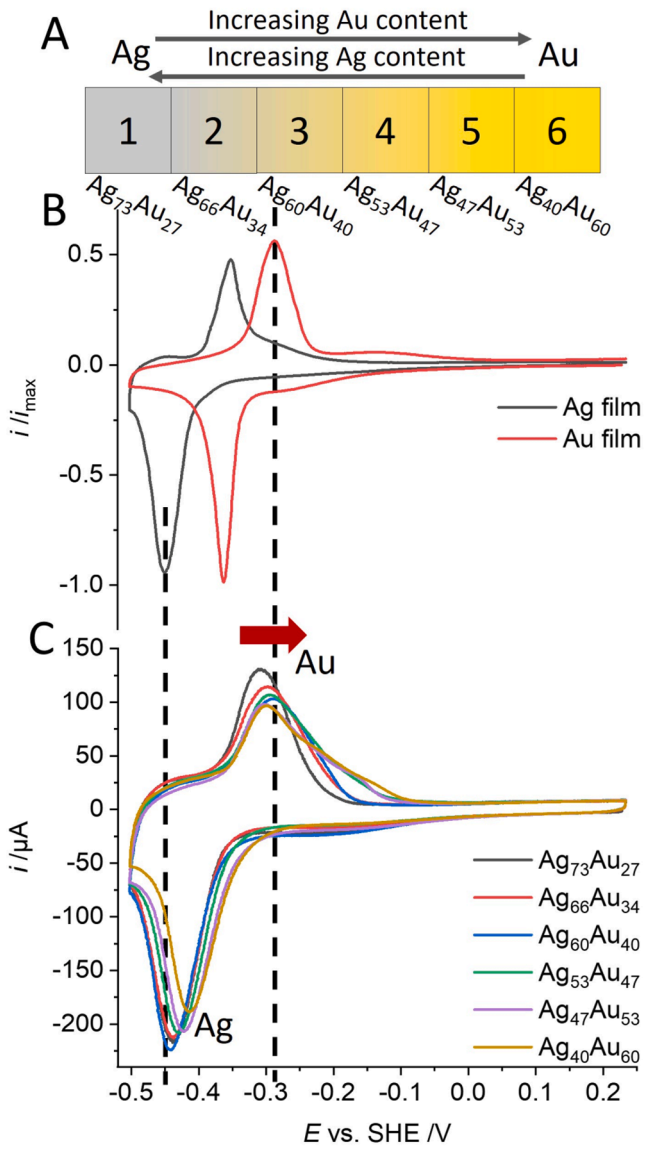

Fig. 3. Sputtered Ag_xAu_y film samples of different compositions used for Pb-UPD and stripping (A). Associated CVs are shown in (C). Pb-UPD and stripping of monometallic films are shown in (B).; Electrolyte: 1 mM $Pb(NO_3)_2$ + 0.1 M NaOH, scan rate = 0.05 V/s.

To rationalise this finding, the energies for Ag-rich and Au-rich surface regions with a Pb adlayer were compared using DFT calculations using VASP (see SI chapter 1) [38–41]. For the calculations we arranged alternating Ag, Au and Pb monolayers in a fcc slab, where the monolayers were oriented perpendicular to the (100) surface. The slabs were then relaxed in plane and perpendicular to the surface. As we repeated a single column of atoms periodically, the surface could not reconstruct or incorporate other defects that one may expect due to the excess of about 20 % between Pb and Au [15,42]. With this basic calculations setup we find that an adlayer of Pb on Au is energetically favoured over an adlayer of Pb on Ag. Irrespective of this, Pb deposition is only observed experimentally at the potential for Pb on Ag deposition, showing that Ag atoms form the outmost surface in aqueous electrolyte.

As discussed above for Ag_xAu_y nanoparticles, this is caused by the larger oxophilicity of Ag [43,44]. Having decorated the surface with Pb, this oxophilicity, however, becomes less relevant and the energetically favourable interaction of Pb and Au, favours motion of Au to the Ag, that is a swapping of position with Ag underneath the adlayer of Pb atoms.

This presence of Au underneath the Pb atoms, then results in the experimentally observed shift of the Pb oxidation peak to a more positive potential, as typical for stripping of Pb from a Au surface.

To estimate the rate of the swap of Ag and Au atoms we performed stripping voltammetry experiments similar to those shown in Fig. 3 at different scan rates ranging from 0.025 V/s to 0.25 V/s (see SI Figure S3). These voltammograms consistently show a single peak for Pb stripping from an Au surface. Instead, two peaks would have been expected if the swapping of Ag and Au was slower than the reversal of potential in the voltametric experiment, since then Pb would have been stripped partially from Ag and partially from Au atoms. Thus, we conclude that the swapping is complete within <0.6 s, which is the time required to scan the potential from the lower vertex potential of −0.5 V vs. SHE to approx. −0.35 V vs. SHE (stripping of Pb from Ag) at the highest scan rate tested. At scan rates faster than 0.25 V/s the Pb-UPD peak shifted strongly towards more negative values, resulting in incomplete formation of the Pb adlayer. This prohibited testing at higher scan rates, as incomplete monolayer formation would prohibit a reliable data analysis.

Furthermore, we observe that the swapping of Ag atoms and Au atoms is reversible within the time scale of the CV experiments as Pb-UPD and stripping peak positions in the first and in consecutive scans are identical, which is shown in the SI Figure S1. Upon removal of Pb from the surface of the Ag_xAu_y film, the increased oxophilicity of Ag atoms causes sub-surface Ag atoms to move back to the outermost surface, that is, the reversal of swapping of Ag and Au atoms in the outermost surface. This is true for both, Ag_xAu_y nanoparticles, and thin film samples.

4. Conclusion

Pb-UPD, often used as an analytical tool to determine electrochemically accessible surface area (ECSA) of macroelectrodes or nano-electrocatalysts is shown here as a method for modifying the composition of the outermost surface of Ag_xAu_y alloy films and nanoparticles [2,3,45]. Conducting CV studies of Pb-UPD, we showed that cathodic peaks reflect the deposition of Pb on Ag, while the Pb stripping occurs from an Au(111)-like surface. We attribute these findings to a rearrangement of the top-most atomic layer. It consists of Ag atoms in the absence of a Pb adlayer and is replaced by Au atoms from surface-near regions when a Pb adlayer is present. The swap of Ag and Au is caused by the replacement of H_2O molecules being in contact with the alloy surface by Pb atoms. While the contact with H_2O favours surface termination by more oxyphilic Ag atoms, in contact with Pb, interaction with the less oxyphilic Au is energetically favoured. This is corroborated by basic DFT calculations that show a preferential interaction of Au with Pb over of Ag with Pb. Repeated Pb deposition and stripping cycles indicate a reversibility of this surface rearrangement. That is, the prevailing Ag-terminated surface is re-established upon stripping of the Pb adlayer.

Further investigations may provide more detailed theoretical simulations of the swapping of surface metals.

The showcased ability to tune surface atom arrangements of alloys by formation of an adlayer is highly interesting, as it provides a so far unexplored route to steer the catalytic activity of multicomponent electrocatalysts, ranging from bi- or trimetallic systems to the emerging field of high entropy alloys catalysts [46,47]. The potential of this concept has been proven for monometallic Au substrates, showing enhanced catalytic activity for the oxygen reduction reaction and glucose oxidation after surface modification by Pb-UPD [48,49].

CRediT authorship contribution statement

Dean-Robin Nettler: Writing – review & editing, Writing – original draft, Methodology, Investigation, Formal analysis, Data curation, Conceptualization. **Jan Clausmeyer:** Writing – original draft, Visualization, Conceptualization. **Alan Savan:** Validation, Formal analysis. **Paolo Cignoni:** Writing – review & editing. **Christian Rurainsky:** Validation, Investigation. **Ralf Drautz:** Formal analysis. **Alfred Ludwig:** Resources. **Kristina Tschulik:** Writing – review & editing, Supervision, Resources, Funding acquisition, Conceptualization.

Declaration of competing interest

The authors declare that they have no known competing financial interests or personal relationships that could have appeared to influence the work reported in this paper.

Acknowledgements

This work is funded by the Deutsche Forschungsgemeinschaft (DFG, German Research Foundation) – SFB 1625, project number 506711657, subprojects C03, A01 and A03. The authors thank Natalia Pukhareva for performing the XRD measurements. The “Zentrum für Grenzflächendominierte Höchstleistungswerkstoffe” (ZGH, Center for Interface-Dominated High Performance Materials) at the Ruhr University Bochum is acknowledged for using its equipment (XRD, SEM). This work was supported by the “Center for Solvation Science” (ZEMOS) funded by the German Federal Ministry of Education and Research BMBF and by the Ministry of Culture and Research of Nord Rhine-Westphalia. K.T. is grateful for the support by the Max Planck Society through the Max Planck Fellowship program. K.T. acknowledges funding from the European Research Council under the European Union’s Horizon 2020 research and innovation programme grant agreement No. 949724 (MITICAT).

Supplementary materials

Supplementary material associated with this article can be found, in the online version, at doi:10.1016/j.electacta.2025.145776.

Data availability

Data will be made available on request.

References

[1] K.A. Stoerzinger, M. Risch, B. Han, Y. Shao-Horn, Recent insights into manganese oxides in catalyzing oxygen reduction kinetics, ACS Catal. 5 (2015) 6021–6031, https://doi.org/10.1021/acscatal.5b01444.
[2] S. Trasatti, O.A. Petrii, Real surface area measurements in electrochemistry, Pure Appl. Chem. 63 (1991) 711–734, https://doi.org/10.1351/pac199163050711.
[3] G. Jarzabek, Z. Borkowska, On the real surface area of smooth solid electrodes, Electrochim. Acta 42 (1997) 2915–2918, https://doi.org/10.1016/S0013-4686(97)00112-6.
[4] R. Woods, Chemisorption At Electrodes: Hydrogen and Oxygen on Noble Metals and Their Alloys, New York, Dekker, 1976.
[5] C. Wei, S. Sun, D. Mandler, X. Wang, S.Z. Qiao, Z.J. Xu, Approaches for measuring the surface areas of metal oxide electrocatalysts for determining their intrinsic electrocatalytic activity, Chem. Soc. Rev. 48 (2019) 2518–2534, https://doi.org/10.1039/C8CS00848E.
[6] M. Escudero-Escribano, A. Verdaguer-Casadevall, P. Malacrida, U. Grønbjerg, B. P. Knudsen, A.K. Jepsen, J. Rossmeisl, I.E.L. Stephens, I. Chorkendorff, Pt5Gd as a highly active and stable catalyst for oxygen electroreduction, J. Am. Chem. Soc. 134 (2012) 16476–16479, https://doi.org/10.1021/ja306348d.
[7] T.J. Schmidt, H.A. Gasteiger, G.D. Stäb, P.M. Urban, D.M. Kolb, R.J. Behm, Characterization of high-surface-area electrocatalysts using a rotating disk electrode configuration, J. Electrochem. Soc. 145 (1998) 2354–2358, https://doi.org/10.1149/1.1838642.
[8] M.P. Green, M. Richter, X. Xing, D. Scherson, K.J. Hanson, P.N. Ross, R. Carr, I. Lindau, In-situ STM studies of electrochemical underpotential deposition of Pb on Au(111), J. Microsc. 152 (1988) 823–829, https://doi.org/10.1111/j.1365-2818.1988.tb01455.x.

[9] U. Schmidt, S. Vinzelberg, G. Staikov, Pb UPD on Ag(100) and Au(100) — 2D phase formation studied by in situ STM, Surf. Sci. 348 (1996) 261–279, https://doi.org/10.1016/0039-6028(95)01000-9.
[10] W. Plieth, Electrochemistry For Material Science, Elsevier, Amsterdam, 2008.
[11] K.-O. Thiel, M. Hintze, A. Vollmer, C. Donner, A new approach on the Cu UPD on Ag surfaces, J. Electroanal. Chem. 621 (2008) 7–12, https://doi.org/10.1016/j.jelechem.2008.03.001.
[12] P. Allongue, F. Maroun, Metal electrodeposition on single crystal metal surfaces mechanisms, structure and applications, Curr. Opin. Solid State Mater. Sci. 10 (2006) 173–181, https://doi.org/10.1016/j.cossms.2007.04.001.
[13] M. Palomar-Pardavé, I. González, N. Batina, New insights into evaluation of kinetic parameters for potentiostatic metal deposition with underpotential and overpotential deposition processes, J. Phys. Chem. B 104 (2000) 3545–3555, https://doi.org/10.1021/jp9931861.
[14] M.P. Green, K.J. Hanson, R. Carr, I. Lindau, STM observations of the underpotential deposition and stripping of Pb on Au(111) under potential sweep conditions, J. Electrochem. Soc. 137 (1990) 3493–3498, https://doi.org/10.1149/1.2086255.
[15] N. Mayet, K. Servat, K.B. Kokoh, T.W. Napporn, Probing the surface of noble metals electrochemically by underpotential deposition of transition metals, Surfaces 2 (2019) 257–276, https://doi.org/10.3390/surfaces2020020.
[16] V. Grasmik, C. Rurainsky, K. Loza, M.V. Evers, O. Prymak, M. Heggen, K. Tschulik, M. Epple, Deciphering the surface composition and the internal structure of alloyed silver-gold nanoparticles, Chem. Eur. J. 24 (2018) 9051–9060.
[17] J. Aldana-González, J. Olvera-García, M.G. Montes de Oca, M. Romero-Romo, M. T. Ramírez-Silva, M. Palomar-Pardavé, Electrochemical quantification of the electro-active surface area of Au nanoparticles supported onto an ITO electrode by means of Cu upd, Electrochem. Commun. 56 (2015) 70–74, https://doi.org/10.1016/j.elecom.2015.04.014.
[18] J.W. Shin, U. Bertocci, G.R. Stafford, Stress response to surface alloying and dealloying during underpotential deposition of Pb on (111)-textured Au, J. Phys. Chem. C 114 (2010) 7926–7932, https://doi.org/10.1021/jp100357r.
[19] J. Yan, Q. Wu, W. Shang, B. Mao, Electrodeposition of Sb on Au(100) at underpotentials: structural transition involving expansion of the substrate surface, Electrochem. Commun. 6 (2004) 843–848, https://doi.org/10.1016/j.elecom.2004.06.007.
[20] M. Huang, J.B. Henry, B.B. Berkes, A. Maljusch, W. Schuhmann, A.S. Bondarenko, Towards a detailed in situ characterization of non-stationary electrocatalytic systems, Analyst 137 (2012) 631–640, https://doi.org/10.1039/c1an15671c.
[21] C. Rurainsky, A.G. Manjón, F. Hiege, Y.-T. Chen, C. Scheu, K. Tschulik, Electrochemical dealloying as a tool to tune the porosity, composition and catalytic activity of nanomaterials, J. Mater. Chem. A 8 (2020) 19405–19413, https://doi.org/10.1039/D0TA04880A.
[22] C. Rurainsky, D.-R. Nettler, T. Pahl, A. Just, P. Cignoni, K. Kanokkanchana, K. Tschulik, Electrochemical dealloying in a magnetic field – Tapping the potential for catalyst and material design, Electrochim. Acta 426 (2022) 140807, https://doi.org/10.1016/j.electacta.2022.140807.
[23] A. Ludwig, Discovery of new materials using combinatorial synthesis and high-throughput characterization of thin-film materials libraries combined with computational methods, Npj Comput. Mater. 5 (2019), https://doi.org/10.1038/s41524-019-0205-0.
[24] A. Ludwig, R. Zarnetta, S. Hamann, A. Savan, S. Thienhaus, Development of multifunctional thin films using high-throughput experimentation methods, Int. J. Mater. Res. 99 (2008) 1144–1149, https://doi.org/10.3139/146.101746.
[25] D.T. Sawyer, Electrochemistry For Chemists, 2nd ed., Wiley, New York, Chichester, 1995.
[26] J. Turkevich, P. Cooper Stevenson, J. Hillier, A study of the nucleation and growth processes in the synthesis of colloidal gold, Discuss. Faraday Soc. (1951) 55–75.
[27] Y. Wang, E. Laborda, B.J. Plowman, K. Tschulik, K.R. Ward, R.G. Palgrave, C. Damm, R.G. Compton, The strong catalytic effect of Pb(II) on the oxygen reduction reaction on 5 nm gold nanoparticles, Phys. Chem. Chem. Phys. 16 (2014) 3200–3208, https://doi.org/10.1039/C3CP55306J.
[28] M. Kamundi, L. Bromberg, E. Fey, C. Mitchell, M. Fayette, N. Dimitrov, Impact of structure and composition on the dealloying of Au x Ag (1–x) alloys on the Nanoscale, J. Phys. Chem. C 116 (2012) 14123–14133, https://doi.org/10.1021/jp301603t.
[29] C. Jeyabharathi, M. Zander, F. Scholz, Underpotential deposition of lead on quasi-spherical and faceted gold nanoparticles, J. Electroanal. Chem. 819 (2018) 159–162, https://doi.org/10.1016/j.jelechem.2017.10.011.
[30] A. Hamelin, Underpotential deposition of lead on single crystal faces of gold, J. Electroanal. Chem. 165 (1984) 167–180, https://doi.org/10.1016/S0022-0728(84)80095-9.
[31] J.W. Schultze, D. Dickertmann, Potentiodynamic desorption spectra of metallic monolayers of Cu, Bi, Pb, Tl, and Sb adsorbed at (111), (100), and (110) planes of gold electrodes, Surf. Sci. 54 (1976) 489–505, https://doi.org/10.1016/0039-6028(76)90239-9.
[32] 16.
[33] N. Eom, M.E. Messing, J. Johansson, K. Deppert, General trends in core-shell preferences for bimetallic nanoparticles, ACS Nano 15 (2021) 8883–8895, https://doi.org/10.1021/acsnano.1c01500.
[34] H. Okamoto, M.E. Schlesinger, E.M. Mueller, Alloy Phase Diagrams, ASM International, 2016.
[35] S. Ristig, O. Prymak, K. Loza, M. Gocyla, W. Meyer-Zaika, M. Heggen, D. Raabe, M. Epple, Nanostructure of wet-chemically prepared, polymer-stabilized silver-gold nanoalloys (6 nm) over the entire composition range, J. Mater. Chem. B 3 (2015) 4654–4662, https://doi.org/10.1039/c5tb00644a.
[36] V. Lubarda, On the effective lattice parameter of binary alloys, Mech. Mater. 35 (2003) 53–68, https://doi.org/10.1016/S0167-6636(02)00196-5.
[37] L. García-Cruz, V. Montiel, J. Solla-Gullón, Shape-controlled metal nanoparticles for electrocatalytic applications, Phys. Sci. Rev. 4 (2019), https://doi.org/10.1515/psr-2017-0124.
[38] G. Kresse, J. Furthmüller, Efficient iterative schemes for ab initio total-energy calculations using a plane-wave basis set, Phys. Rev. B Condens. Matter 54 (1996) 11169–11186, https://doi.org/10.1103/PhysRevB.54.11169.
[39] G. Kresse, J. Hafner, Ab initio molecular dynamics for open-shell transition metals, Phys. Rev. B Condens. Matter 48 (1993) 13115–13118, https://doi.org/10.1103/PhysRevB.48.13115.
[40] G. Kresse, J. Furthmüller, Efficiency of ab-initio total energy calculations for metals and semiconductors using a plane-wave basis set, Comput. Mater. Sci. 6 (1996) 15–50, https://doi.org/10.1016/0927-0256(96)00008-0.
[41] J.P. Perdew, K. Burke, M. Ernzerhof, Generalized gradient approximation made simple, Phys. Rev. Lett. 77 (1996) 3865–3868, https://doi.org/10.1103/PhysRevLett.77.3865.
[42] M.G. Samant, M.F. Toney, G.L. Borges, L. Blum, O.R. Melroy, Grazing incidence x-ray diffraction of lead monolayers at a silver (111) and gold (111) electrode/electrolyte interface, J. Phys. Chem. 92 (1988) 220–225, https://doi.org/10.1021/j100312a047.
[43] K.P. Kepp, A quantitative scale of oxophilicity and thiophilicity, ACS Appl. Energy Mater. 55 (2016) 9461–9470, https://doi.org/10.1021/acs.inorgchem.6b01702.
[44] N. Lee, H.Y. Jang, K. Shim, S.-M. Jung, J. Lee, S.-H. You, H.S. Kang, J.K. Kim, S. Back, Y.-T. Kim, Enhanced activity and selectivity for electrochemical CO 2 reduction through water activation by oxophilic metal deposited on Ag, ACS Appl. Energy Mater. 6 (2023) 4413–4421, https://doi.org/10.1021/acsaem.3c00530.
[45] P. Cignoni, P. Hosseini, C. Kaiser, O. Trost, D.-R. Nettler, L. Trzebiatowski, K. Tschulik, Validating electrochemical active surface area determination of nanostructured electrodes: surface oxide reduction on AuPd nanoparticles, J. Electrochem. Soc. 170 (2023) 116505, https://doi.org/10.1149/1945-7111/ad09f8.
[46] T. Löffler, A. Ludwig, J. Rossmeisl, W. Schuhmann, What makes high-entropy alloys exceptional electrocatalysts? Angew. Chem. Int. Ed. Engl. 60 (2021) 26894–26903, https://doi.org/10.1002/anie.202109212.
[47] Y. Xin, S. Li, Y. Qian, W. Zhu, H. Yuan, P. Jiang, R. Guo, L. Wang, High-entropy alloys as a platform for catalysis: progress, challenges, and opportunities, ACS Catal. 10 (2020) 11280–11306, https://doi.org/10.1021/acscatal.0c03617.
[48] F. Calle-Vallejo, M.T.M. Koper, A.S. Bandarenka, Tailoring the catalytic activity of electrodes with monolayer amounts of foreign metals, Chem. Soc. Rev. 42 (2013) 5210–5230, https://doi.org/10.1039/c3cs60026b.
[49] S. Hebié, T.W. Napporn, K.B. Kokoh, Beneficial promotion of underpotentially deposited lead adatoms on gold nanorods toward glucose electrooxidation, Electrocatalysis 8 (2017) 67–73, https://doi.org/10.1007/s12678-016-0343-9.